Nonlinear Elimination of Spin-Exchange Relaxation of High Magnetic Moments

Or Katz,[1,3] Mark Dikopoltsev,[2,3] Or Peleg,[3] Moshe Shuker,[2,3] Jeff Steinhauer,[2] and Nadav Katz[1]

[1]*Racah Institute of Physics, The Hebrew University of Jerusalem, Jerusalem 91904, Israel*
[2]*Department of Physics, Technion, Israel Institute of Technology, Haifa 32000, Israel*
[3]*RAFAEL, Science Center, Rafael Ltd., Haifa 31021, Israel*

(Received 29 April 2013; published 26 June 2013)

Relaxation of the Larmor magnetic moment by spin-exchange collisions has been shown to diminish for high alkali densities, resulting from the linear part of the collisional interaction. In contrast, we demonstrate both experimentally and theoretically the elimination of spin-exchange relaxation of high magnetic moments (birefringence) in alkali vapor. This elimination originates from the nonlinear part of the spin-exchange interaction, as a scattering process of the Larmor magnetic moment. We find counterintuitively that the threshold magnetic field is the same as in the Larmor case, despite the fact that the precession frequency is twice as large.

DOI: 10.1103/PhysRevLett.110.263004 PACS numbers: 33.35.+r, 07.55.Ge, 32.60.+i, 32.80.Xx

Atomic relaxation mechanisms in vapor physics limit the precision and performance of many spectroscopic measurements. For example, the performance of atomic clocks [1] and sensitive magnetometers [2] is determined by these relaxations. The dominant ground state relaxation mechanism is induced by spin-exchange collisions of alkali atoms [3,4]. However, it was found that at high atomic densities the Larmor (dipolar) coherence, associated with any two nearest Zeeman splitted levels, improves significantly with its frequency being slowed down [5,6]. This unique effect is known as the spin-exchange relaxation free (SERF) effect since the relaxation due to spin-exchange collisions is completely suppressed and only next-order relaxation processes, such as the power broadening of a pumping laser, become apparent. This effect sets the stage for ultrasensitive vapor based magnetometery schemes [7].

Since alkali vapor is essentially a multilevel quantum system, in many coherent phenomena various orders of atomic coherence are involved, each describing the coupling strength between one energy level and another. The use of high orders of coherence introduced phenomena such as nonlinear magneto-optical rotation [8] and had a great contribution in improving magnetometery schemes [9]. Although the high orders of coherence are also relaxed by spin-exchange collisions, up to this point only the lowest order coherence (dipolar) was studied experimentally and theoretically at high atomic densities while the higher orders of coherence in this regime were completely avoided.

In this Letter we demonstrate experimentally that the birefringent coherence, associated with any two next-nearest Zeeman splitted levels, also experiences SERF in the low magnetic field regime. We further explain both numerically and analytically the origin of this effect and deduce the main characteristics of this phenomena such as its decoherence rate, oscillation frequency, and the magnetic field threshold of the SERF regime. Magnetic moment orders higher than the birenfringence are also treated, exhibiting a cascaded process leading to SERF. Finally, we show that ultra-sensitive magnetometers, based on the birefringent coherence, have twice the bandwidth of the Larmor magnetometer with the same sensitivity.

To measure the Larmor and birefringent coherences a pump-probe scheme is utilized (Fig. 1), where the pump polarizes the atomic vapor, and the absorption of the probe by the atoms is measured. This absorption is described by the susceptibility of the medium, which is in turn constructed by means of the different magnetic moments of the atomic density matrix. A proper measurement of the different moments is designed by choosing the relevant magnetic orders of the susceptibility.

The different orders of ground state coherence can be described by expanding the ground state density matrix ρ to its different multiplets $\rho_{LM}(FF')$ [10]. Each multiplet describes the coherence between the hyperfine levels F and F' with L polarization moment distribution. The lowest three multiplets are the isotropic ($L = 0$), dipolar ($L = 1$), and birefringent ($L = 2$) multiplets describing the population of the hyperfine levels F, F', the dipole moments, and

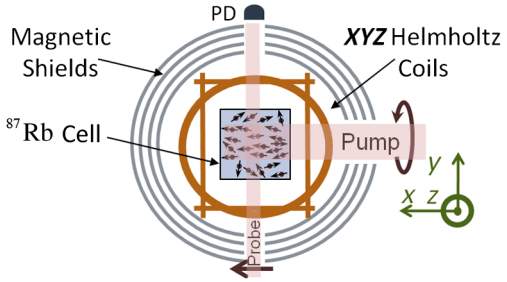

FIG. 1 (color online). Experimental setup for the birefringent measurement. The cell is initially polarized by a σ_+ pumping beam. Then, the absorption of a π probe is measured at a free induction decay of the vapor in the presence of an applied magnetic field B_z.

the quadrupole moments of their Zeeman sublevels, respectively. The M quantum number denotes the energy level spacing of the Zeeman splitting $M\hbar\omega_B$, and is associated with the natural frequency $M\omega_B$. This expansion is of special significance since single-photon interactions, being described by the complex susceptibility observable χ, involve solely the lowest three atomic multiplets [11]. All coherences satisfy $-L \leq M \leq L$ and we identify the $L = |M| = 1$ as the Larmor coherence and $L = |M| = 2$ as the birefringent one. These coherences can be measured by monitoring I_l, the intensity of a weak probe light beam after it propagates a distance l of alkali vapor [11]

$$I_l = I_0 \exp\Big[-2\pi l \sum_{ij} e_i^* \,\mathrm{Im}(\langle\chi_{ij}\rangle) e_j\Big], \tag{1}$$

where I_0 is the probe intensity, e_i is the electric polarization vector of the probe, with

$$\langle\chi_{ij}\rangle = \sum_{LMFF'} \chi^{ij}_{LMFF'} \rho_{LM}(FF'). \tag{2}$$

Here i, j are the spatial Cartesian coordinates and $\chi^{ij}_{LMFF'}$ are the relative strength coefficients [11,12]. From Eqs. (1) and (2) the absorption of a linear probe decays exponentially in time, with a decay rate proportional to the birefringent multiplet ρ_{22}.

We measure the birefringent coherence by monitoring the absorption of a linear probe and the Larmor coherence with a circular probe. We use a 17^3 mm^3 cubic cell with ^{87}Rb, heated to temperature $T = 111.5°$ (atomic density $\sim 10^{13}$ cm^{-3}). We reduce the collision rate with the cell walls by introducing 90 torr of N_2 buffer gas. We control the applied magnetic field by shielding the cell with μ-metal cylinders and three perpendicular Helmholtz coils. A collimated distributed feedback laser beam with a wide Gaussian profile (23 mm width) optically pumps the atoms with circularly polarized light and effective pumping power (0.97 mW) much lower than the saturation intensity. Then, the pumping beam is switched off and a magnetic field $B\hat{z}$ is applied. As a result, the alkali spins start to precess around the magnetic field. This precession decays due to the different relaxation mechanisms. We probe this precession by measuring the absorption of a weak narrow beam (3 mm width with a power of 2.5 μW). The Larmor coherence is probed in the $F_g = 2$ to $F_e = 1$ $D1$ transition. To minimize the isotropic (T_1) probed part from the birefringent part we 1 GHz red-detune the probe. The pressure of the buffer gas was chosen such that the excited-state hyperfine levels are still resolved, and the birefringent strengths χ^{ij}_{2MFF} are observable [13].

A typical π absorption (birefringent) measurement is shown in Fig. 2 for an applied magnetic field of 28 nT in the low magnetic field regime. A measurement of the Larmor absorption for the same parameters is shown for reference. The measured birefringent signal oscillates with frequency ω^{br} which is twice the frequency of the measured Larmor signal ω^{lr}. The decoherence rates and frequencies were determined by fitting each signal to the simple model $f = Ae^{-(t/T_1)} + Ce^{-\Gamma_0 t}\cos(\omega_0 t)$, assuming that both ω_0 and Γ_0 are time independent (a negligible dependence less than 8% was observed). The fit was performed for times longer than $t_0 = 300$ μsec satisfying $t_0 \gg R_{\mathrm{SE}}^{-1}$, where $R_{\mathrm{SE}} \approx 100$ μsec is the mean spin-exchange rate [6], to eliminate other rapidly decaying moments.

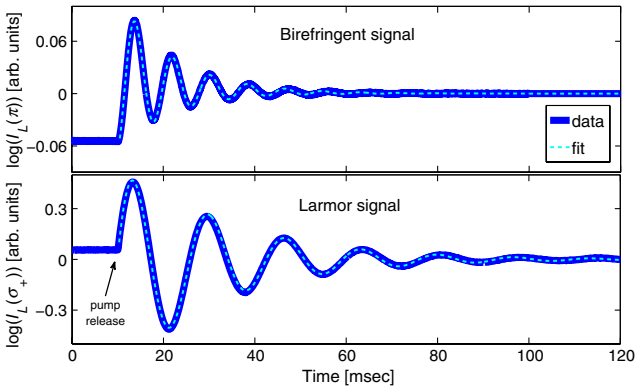

FIG. 2 (color online). A typical measurement of the oscillation and decay of the Larmor and birefringent coherences (500 averages). The birefringent signal oscillates at twice the Larmor frequency and decays twice as fast. The fit to each of the signals is shown (dotted curve).

We find that the birefringent decoherence rate $\Gamma_0^{\mathrm{br}}(B)$ decreases significantly by the decrease of the magnetic field as shown qualitatively in Fig. 3 and quantitatively in Fig. 4. These graphs indicate the effect of rapid spin-exchange collisions on both the Larmor and the birefringent coherences. At high magnetic fields, the decoherence rate is limited by the high spin-exchange collision rate R_{SE} and approaches a constant value. By decreasing the magnetic field, the decoherence rate associated with spin-exchange collisions decreases, approaching quadratically to the lower plateau in the low magnetic field regime. The lower plateau is determined by other polarization (T_1) decoherence processes such as the diffusion time of the atoms to the cell walls. In that sense, the decoherence rate

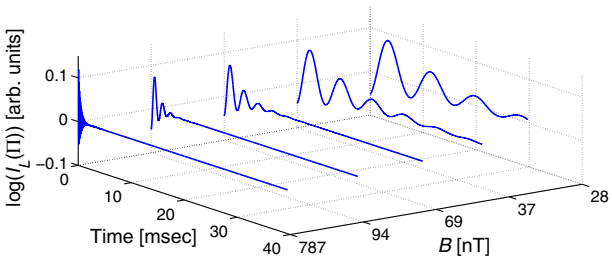

FIG. 3 (color online). Measurement of the transition into the SERF regime of the birefringent coherence. The decoherence rate decreases significantly by decreasing the applied magnetic field.

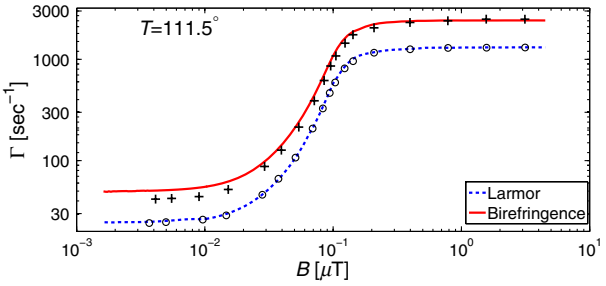

FIG. 4 (color online). The measured magnetic field dependence of the decoherence rates $\Gamma_0^{\mathrm{lr}}(B)$ (circle) and $\Gamma_0^{\mathrm{br}}(B)$ (plus). It is apparent that both the Larmor and birefringent signals experience SERF at the same magnetic field threshold. The birefringent decoherence rate is twice the Larmor decay rate. The simulated decoherence rates of the Larmor (dashed) and the birefringent (solid) coherences are shown.

is now T_1 limited and the spin-exchange relaxation is eliminated. In this regime it is found that $\Gamma_0^{\mathrm{br}}(B)$ satisfies

$$\Gamma_0^{\mathrm{br}}(B) \cong 2\Gamma_0^{\mathrm{lr}}(B) \tag{3}$$

yielding a scaled SERF narrowing for the birefringent decoherence rate $\Gamma_0^{\mathrm{br}}(B)$ relative to the Larmor decoherence rate $\Gamma_0^{\mathrm{lr}}(B)$. Since the measured birefringent signal is associated with the second harmonic of the Larmor frequency, we identify this process as a nonlinear one [14] and will later explain its nature. We thus conclude that the birefringent coherence experiences the nonlinear SERF effect at the same magnetic field threshold of the Larmor coherence with its frequency and decoherence rate doubled.

To verify that the model of spin-exchange relaxations is valid for the measurements, numerical ground state simulations are performed, considering the following Liouville equation [7]

$$\frac{d\rho}{dt} = A_{\mathrm{hfs}}\frac{[\mathbf{I}\cdot\mathbf{S},\rho]}{i\hbar} + \omega_B\frac{[S_z,\rho]}{i\hbar} + R_{\mathrm{SE}}(4\alpha\mathbf{S}\langle\mathbf{S}\rangle - \mathbf{A}\cdot\mathbf{S}) - R_{\mathrm{SD}}\mathbf{A}\cdot\mathbf{S}, \tag{4}$$

where $\mathbf{I}$ and $\mathbf{S}$ are the nuclear and electronic spin observables, A_{hfs} is the hyperfine coupling constant of ^{87}Rb, ω_B is the bare electron precession frequency and R_{SD} is the spin-destructing collision rate. The operators α and $\mathbf{A}$ are the nuclear and electronic parts of the density matrix $\rho = \alpha + \mathbf{A}\cdot\mathbf{S}$ [6]. Hyperfine coherences ($F \neq F'$) are neglected to improve the simulation runtime [15].

The predictions of the numerical model are plotted in Fig. 4. We used a single fitting parameter ($R_{\mathrm{SD}} = 147\ \mathrm{sec}^{-1}$), determined by fitting the decoherence rate of the Larmor coherence at low magnetic fields. The birefringence is plotted using no free parameters. The simulations also yield the slight time dependence of the measured frequencies and decoherence rates, resulting from the relaxation of the mean spin polarization. Therefore, the subscript "0" denotes the values of the decoherence rates Γ_0^{lr}, Γ_0^{br} in the low-polarization regime. Evidently, the simulations verify that all the processes governing the birefringent coherence are included in Eq. (4). Furthermore, the main observations of the SERF magnetic field threshold, the decoherence rate and precession frequency are well described by the simulations.

These results are surprising in two aspects. First, one would expect the birefringent coherence to experience SERF at magnetic fields satisfying $\omega_0^{\mathrm{br}} = 2\omega_0^{\mathrm{lr}} \lesssim R_{\mathrm{SE}}$ while de facto it satisfies the same condition as the Larmor coherence $\omega_0^{\mathrm{lr}} \lesssim R_{\mathrm{SE}}$. Second, Eq. (3) is rather surprising since neither a spin vector model [15] nor a motional narrowing-based model [6] can describe it. These models are based on the linearized spin-exchange interaction, neglecting nonlinear terms arising from the interaction with the mean spin polarization. In the following, we show that the dynamics of the birefringent coherence relies entirely on this nonlinear mechanism. To examine this nonlinearity using perturbation analysis, we rephrase Eq. (4) using the super-operator formalism [6]

$$\frac{d\rho}{dt} = (W + Z + E + Q(\rho))\rho, \tag{5}$$

where W denotes the hyperfine interaction, Z denotes the interaction of the external magnetic field with the electron spin, and E and $Q(\rho)$ denote the linear and nonlinear terms of the spin-exchange relaxation. For simplicity we neglect the spin destruction interaction. To describe Eq. (5) in the interaction picture we use the basis of eigenoperators $|LM\pm\rangle$ (associated with the magnetic L, M multiplets) of the linear super-operator $W + Z + E$. These eigenoperators were first calculated in [6] for the multiplets $L = 0, 1$. The calculation is extended for $L > 1$ in [16]. In the linear theory, ρ satisfies

$$\rho(t)|^{\mathrm{linear}} = \sum_{LM\pm}\rho_{LM\pm}(0)e^{\lambda_\pm^{LM}t}|LM\pm\rangle, \tag{6}$$

where the magnetic eigenvalues $\lambda_\pm^{LM}$ describe the dynamics of ρ completely. In the low magnetic field regime ($\omega_0 \lesssim R_{\mathrm{SE}}$) these eigenvalues are given by [16]

$$\lambda_\pm^{LM} \approx \pm\frac{ib_L M}{2c_L}\omega_0 - R_{\mathrm{SE}}(a_L \mp c_L) - \mathcal{O}\left(\frac{\omega_0^2}{R_{\mathrm{SE}}}\right), \tag{7}$$

where $\omega_0 = \omega_B/(2I+1)$ is the slowed down Larmor frequency and the coefficients a_L, b_L, c_L are given in [16].

Using the $|LM\pm\rangle$ basis, we transform Eq. (5) to the interaction picture to include the nonlinear interaction $Q(\rho)\rho$

$$\rho_{LM\pm}(t) = \rho_{LM\pm}(0)e^{\lambda_\pm^{LM}t} + 2R_{\mathrm{SE}}\sum_{l,m,k,\pm'}Q\{k\}_{lm\pm'}^{LM\pm} \times\int e^{\lambda_\pm^{LM}(t-t')}\rho_{lm\pm'}(t')\langle S_k\rangle dt', \tag{8}$$

where the super-operator Q is given in the magnetic multiplets representation $|LM\pm\rangle$ by [17]

$$\langle LM \pm |Q| lm \pm' \rangle = 2R_{\mathrm{SE}} \sum_{k=-1}^{1} Q\{k\}_{lm\pm'}^{LM\pm} \langle S_k \rangle. \quad (9)$$

Here, k denotes spherical coordinates and the coefficients $Q\{k\}_{lm\pm'}^{LM\pm}$ are defined by angular momentum transformations in [16]. We note that $Q\{k\}_{lm\pm'}^{LM\pm}$ satisfy the selection rules implied by the condition

$$Q\{k\}_{lm\pm'}^{LM\pm} \propto C(l, 1; mk; LM)(1 - \delta_{l0}), \quad (10)$$

where C is the Clebsch-Gordan coefficient. By Eq. (9), the typical rate of $Q\{k\}$ is $2R_{\mathrm{SE}}\langle S_k \rangle$. Since this rate satisfies $2R_{\mathrm{SE}}\langle S_k \rangle \leq R_{\mathrm{SE}}$, in the low-polarization regime, one can approximate the contribution of Q by using a time-dependent perturbation theory. This method is applied by approximating $Q(\rho) \approx Q(\rho|^{\mathrm{linear}})$ in Eq. (8). In the low magnetic field regime of the linear theory [Eq. (7)], the only nonvanishing components of $\rho_{lm\pm}$ for long times $t \gg R_{\mathrm{SE}}^{-1}$ are

$$\rho_{lm\pm}(t)|_{t \gg R_{\mathrm{SE}}^{-1}}^{\mathrm{linear}} \rightarrow \rho_{lm+}(t_0) e^{\lambda_+^{lm}(t-t_0)} (\delta_{l0} + \delta_{l1}), \quad (11)$$

where t_0 is some initial time satisfying $t_0 \gg R_{\mathrm{SE}}^{-1}$. Applying the last equation to $\langle S_k \rangle$ one obtains

$$\langle S_k(t) \rangle|_{t \gg R_{\mathrm{SE}}^{-1}}^{\mathrm{linear}} \rightarrow \langle S_k(t_0) \rangle e^{\lambda_+^{1k}(t-t_0)}. \quad (12)$$

The $L \neq 1$ Zeeman multiplets are given by substituting the linear solutions [Eqs. (11) and (12)] in Eq. (8). Performing integration for times $t \gg R_{\mathrm{SE}}^{-1}$ yields

$$\rho_{LM\pm}(t) \approx \sum_{m,k=-1}^{1} \frac{2R_{\mathrm{SE}}\langle S_k(t_0) \rangle \rho_{1m+}(t_0)}{-\lambda_{\pm}^{LM} + \lambda_+^{1m} + \lambda_+^{1k}} \times Q\{k\}_{1m+}^{LM\pm} e^{(\lambda_+^{1m} + \lambda_+^{1k})(t-t_0)}, \quad (13)$$

where rapid decaying terms (with typical decoherence rate of $\Gamma \approx R_{\mathrm{SE}}$) are neglected. Considering the Clebsch-Gordan coefficient in Eq. (10), the selection rule $k + m = M$ is obtained. Introducing this condition to the birefringent multiplets $L = |M| = 2$ in Eq. (13) one obtains

$$\rho_{2M\pm}(t) \approx \left(\frac{2\langle S_k(t_0) \rangle \rho_{1k+}(t_0)}{a_2 \mp c_2} Q\{k\}_{1k+}^{2M\pm} \right) e^{2\lambda_+^{1k}(t-t_0)} \quad (14)$$

for $k = M/2$. Thus, the evolution of the birefringent multiplets is determined by a single exponent. We can now identify the new birefringent eigenvalue $\lambda^{2M}|_{M=\pm 2}^{\mathrm{nonlinear}} \equiv \pm i\omega_0^{\mathrm{br}} - \Gamma_0^{\mathrm{br}}$ with

$$\lambda^{2M}|_{M=\pm 2}^{\mathrm{nonlinear}} = 2\lambda_+^{1M}|_{M=\pm 1}^{\mathrm{linear}}. \quad (15)$$

Since the Larmor multiplets with eigenvalues $\lambda_+^{1k}|_{k=\pm 1}^{\mathrm{linear}} = \pm i\omega_0^{\mathrm{lr}} - \Gamma_0^{\mathrm{lr}}$ experience SERF, we find that the birefringent multiplets also experience SERF with both the frequency and the decoherence rate doubled, in complete correspondence with the experiment and simulations. However, the mechanism for this spin-exchange relaxation elimination is completely different from the elimination introduced by the linear theory. The emergence of the birefringent $M = \pm 2$ coherence can be interpreted as an induced nonlinear scattering of the Larmor coherence (ρ_{1k+}) by the effective mean field potential $Q(\langle S_k \rangle)|^{\mathrm{linear}}$ [Eq. (8)]. Both the Larmor coherence and the mean electronic spin $\langle \mathbf{S} \rangle$ experience the linear SERF effect but their coupling induces the birefringence. Therefore, the birefringent SERF magnetic threshold $R \gtrsim \omega_0^{\mathrm{lr}}$ is the same as the Larmor threshold. Moreover, the observed birefringent doubled slowed-down frequency results from the time dependence of the scattering rate ($\langle \mathbf{S}(t) \rangle$) and not from a statistical mixture of birefringent precession of different hyperfine levels. This is the reason why this effect cannot be explained in terms of the linear model and is therefore designated as the nonlinear SERF effect.

Although resulting from a nonlinear interaction, it should be noted that these eigenvalues are not ρ or $\langle S_k \rangle$ dependent, since $\langle S_k \rangle$ is mainly dominated by $\langle S_k(t) \rangle|^{\mathrm{linear}}$. However, by considering higher order terms in the perturbation expansion [Eq. (8)] beyond the low-polarization regime, polarization-dependent corrections of the slowing down factor $q(P)$ can be obtained [18]. Furthermore, these higher order perturbation terms induce the scattering of higher order moments ($L > 2$). Following the selection rules of Q in Eq. (10), any induced moment L is scattered only by a lower moment $L - 1$. Thus, by iterating the perturbative analysis, one can show that these higher moments follow a cascade of nonlinear SERF scattering. The measurement of these higher moments is more complicated [13], and will be treated in a future publication.

For a given magnetic field, the birefringent coherence precesses twice as fast as the Larmor coherence. Thus, a birefringent based magnetometer will have twice the bandwidth of a Larmor-based magnetometer. The fundamental sensitivity [7] ratio between a birefringent based magnetometer and a Larmor-based magnetometer would be $\sqrt{1/(2\eta_{\mathrm{br}})}$ where $\eta_{\mathrm{br}} = N_{\mathrm{br}}/N_{\mathrm{lr}}$ is the relative birefringent number of oscillators with respect to the Larmor number of oscillators. This can be approximated by $\eta_{\mathrm{br}} \approx |\rho_{22+}/\rho_{11+}|$. Using Eq. (14), one can estimate $\eta_{\mathrm{br}} \approx 1$ for moderate polarizations. Thus, the fundamental sensitivity of a birefringent based magnetometer will have the same sensitivity as a Larmor-based magnetometer.

In conclusion, we have demonstrated experimentally and theoretically that the birefringent coherence experiences nonlinear SERF at low magnetic fields, with the same magnetic field threshold but with doubled frequency and decoherence rate. We have shown that the birefringence coherence originates from a nonlinear scattering of the Larmor coherence by the mean electronic spin of the vapor, and that other higher orders of coherence experience a similar scattering process. Finally, we have shown that birefringent based magnetometers will have the same sensitivity as a Larmor based magnetometers with twice the bandwidth.

[1] J. Vanier, Appl. Phys. B **81**, 421 (2005).
[2] D. Budker and M. V. Romalis, Nat. Phys. **3**, 227 (2007).
[3] E. M. Purcell and G. B. Field, Astrophys. J. **124**, 542 (1956).
[4] J. P. Wittke and R. H. Dicke, Phys. Rev. **103**, 620 (1956).
[5] W. Happer and H. Tang, Phys. Rev. Lett. **31**, 273 (1973).
[6] W. Happer and A. C. Tam, Phys. Rev. A **16**, 1877 (1977).
[7] J. C. Allred, R. N. Lyman, T. W. Kornack, and M. V. Romalis, Phys. Rev. Lett. **89**, 130801 (2002).
[8] D. Budker, W. Gawlik, D. F. Kimball, S. M. Rochester, V. V. Yashchuk, and A. Weis, Rev. Mod. Phys. **74**, 1153 (2002).
[9] D. Budker, D. F. Kimball, S. M. Rochester, V. V. Yashchuk, and M. Zolotorev, Phys. Rev. A **62**, 043403 (2000).
[10] W. Happer, Rev. Mod. Phys. **44**, 169 (1972).
[11] B. S. Mathur, H. Y. Tang, and W. Happer, Phys. Rev. A **2**, 648 (1970).
[12] W. Happer and B. Mathur, Phys. Rev. **163**, 12 (1967)
[13] M. Auzinsh, D. Budker, and S. M. Rochester, Phys. Rev. A **80**, 053406 (2009).
[14] R. W. Boyd, *Nonlinear Optics* (Academic Press, New York, 2003), 2nd ed., Chap. 3.
[15] I. M. Savukov and M. V. Romalis, Phys. Rev. A **71**, 023405 (2005).
[16] See Supplemental Material at http://link.aps.org/supplemental/10.1103/PhysRevLett.110.263004 for a comprehensive description of the linear theory and the representation of Q.
[17] The neglect of the hyperfine multiplets is discussed in [16].
[18] This dependence was demonstrated for the Larmor coherence in [15].